Ceramics International 50 (2024) 9089–9095

Contents lists available at ScienceDirect

Ceramics International

journal homepage: www.elsevier.com/locate/ceramint

Narrow-angle privacy protection based on anomalous propagation characteristics at epsilon-near-zero threshold frequency of $YaBa_2Cu_3O_7$ ceramic material

Bao-Fei Wan, Hai-Ning Ye, Yi-Ming Ma, Hai-Feng Zhang *

College of Electronic and Optical Engineering & College of Flexible Electronics (Future Technology), Nanjing University of Posts and Telecommunications, Nanjing, 210023, China

ARTICLE INFO

Handling Editor: Dr P. Vincenzini

Keywords:
Optical privacy protection
Anomalous propagation characteristics
Epsilon-near-zero threshold frequency
$YaBa_2Cu_3O_7$ ceramic material

ABSTRACT

In this paper, an optical privacy protection (OPP) device suitable for the TM wave by taking advantage of the anomalous propagation characteristics (APC) at epsilon-near-zero threshold frequency (ETF) of $YaBa_2Cu_3O_7$ ceramic material coupled with the anti-reflection structure (AFS) is proposed. The APC at ETF can be used to provide angular transparency windows with highly selective properties in both the frequency and angle domains, while the AFS facilitates improving transmittance. Considering the limitation of temperature regulation, to control the size of the transmission window within a narrow range, prisms are introduced as the background medium. It is displayed that the proposed structure has a transmittance of more than 93 % in the region of −30°–30°, while the transmittance is close to 0 beyond −40° or 40°. The OPP covers 405–790 THz, involving the entire visible light region, and has a rectangle coefficient consistently exceeding 0.97. Taking the current process error into consideration, the thickness errors of ±5 % exert little effect on the result.

1. Introduction

With the widespread use of display equipment, there have been various new display requirements and applications proposed, the most common of which are mobile phones and laptops. In many specific public places, to protect personal privacy and major property issues, the confidentiality of display information is increasing, which is the reason that the narrow-view display technology has attracted extensive attention from industry and researchers in recent years [1,2]. Hitherto, the main optical privacy protection (OPP) technology is to coat the surface of the display with a film structure with an anti-peephole function [3–6]. The core of the anti-peephole film structure is the optical technology of ultra-fine blinds. Under the action of this optical technology, the light in the front of the screen is only blocked by the narrowest area of the blade, with the highest transmission rate and the strongest visibility. With the angle tilting, the area of the light blocked by the blade becomes larger, with the transmission rate gradually decreasing, resulting in the gradual dimming of the screen, which can effectively prevent peeping. However, this technology also has its own flaws. On the one hand, due to the inherent limitations of the shutter structure, the transmission rate is less than 70 %, which affects the health of the eyes. On the other hand, the structure has a low rectangle coefficient (*RC*) and a large angular transition range from the visible area to the protected area, about 20°, which limits the security of privacy protection. Therefore, the existence of these two shortcomings also makes the OPP structure not widely used for a long time.

The appearance of photonic crystals (PCs) multi-layer structure [7–10] provides the possibility to solve the above two problems. In 2016, Iizuka et al. [11] proposed to use photonic band-gap properties to achieve angular selection structures with high transmittance and high *RC*, but with a bandwidth of only a few terahertz (THz). In 2023, Wan et al. [12], using the epsilon-near-zero characteristics of single negative media, also realized a high transmission device with high selection characteristics, working in the gigahertz band, which is also not applicable to OPP. Consequently, to highlight the advantages of PCs structure in the design of OPP devices, overcoming the frequency band problem is the most critical [13–16], and the relevant reports have seldom been reported.

The emergence of superconductor ceramic materials provides new vitality for enhancing the flexibility of PCs. Based on the temperature

* Corresponding author. College of Electronic and Optical Engineering & College of Microelectronics, Nanjing University of Posts and Telecommunications, Nanjing, 210023, China.
E-mail address: hanlor@163.com (H.-F. Zhang).

https://doi.org/10.1016/j.ceramint.2023.12.222
Received 24 August 2023; Received in revised form 15 November 2023; Accepted 16 December 2023
Available online 18 December 2023

control characteristics and low loss characteristics of superconductors, superconducting PCs show unique advantages in the design of filters, sensors, omnidirectional reflectors, and other fields [17–19]. In particular, Chen et al. [20] reported anomalous propagation characteristics (APC) of superconductors near epsilon-near-zero threshold frequency (ETF). For traditional epsilon-near-zero materials, electromagnetic waves are usually transmitted at ETF, while for superconductors, abnormal reflections occur at ETF. Although their research focuses on the frequency domain, it is predictable that APC will also exist if the research is transferred to the angle domain. This undoubtedly provides a new idea for the research angle selectivity.

In this paper, the APC at ETF of $YaBa_2Cu_3O_7$ ceramic material is utilized to realize the OPP structure for the TM wave. Combining the characteristics of the dielectric-frequency response of superconducting materials with the anti-reflection structure (AFS), the problem of insufficient working bandwidth of PCs structure is overcome. In addition, the high transmission and large *RC* of the PCs structure are used to improve the defects of the traditional ultra-fine blinds technology. To adjust the visualization angle, prism structures are also introduced. It is shown that in the visible light band of 405~790 THz, the transmittance is higher than 93 %, and *RC* is higher than 0.97. The visible area is within ±30°, with less than 10° of the transition area, and the transmission of the area outside ±40° tends to 0, achieving privacy protection.

2. Structure design and investigation

In Fig. 1, the whole arrangement is in the order of $(YaBa_2Cu_3O_7{\cdot}SiO_2)^2{\cdot}YaBa_2Cu_3O_7{\cdot}(SiO_2{\cdot}YaBa_2Cu_3O_7)$. The middle $YaBa_2Cu_3O_7$ ceramic layer is the host structure, and the $(YaBa_2Cu_3O_7{\cdot}SiO_2)^2$ and $(SiO_2{\cdot}YaBa_2Cu_3O_7)$ on both sides are AFSs. The prism is a kind of glass N-BK7 with a refractive index of 1.51 [21], serving as the background medium. The refractive index and thickness of SiO_2 are 1.45 and 26 nm [22], respectively. For the $YaBa_2Cu_3O_7$ ceramic material, the dielectric function is described by the two-fluid model and London local electrodynamics. When the temperature is lower than the critical temperature, the superconductor can be regarded as lossless, and the dielectric function model can be described as [22,23]:

$$\varepsilon = 1 - \frac{1}{\omega^2 \mu_0 \varepsilon_0 \lambda_L^2} \tag{1}$$

where, λ_L is the temperature-dependent London penetration length which is given by Refs. [22,23],

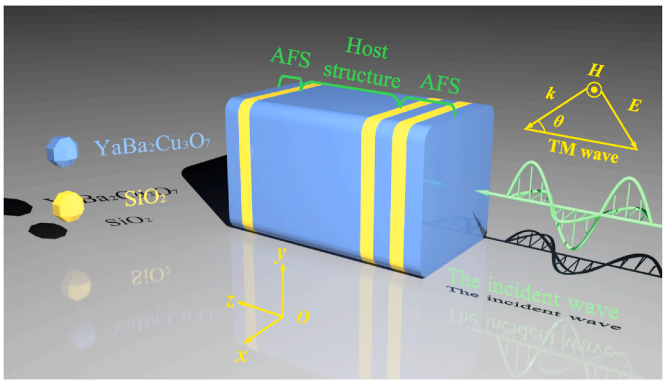

Fig. 1. The proposed OPP diagram. The incident wave propagates in the direction of $+z$ and the angle θ between the wave vector k and the z axis. The incident wave is the TM wave. Since the direction of the magnetic field is perpendicular to the direction of propagation, there is no magnetic component in the direction of propagation, but there is a magnetic component.

$$\lambda_L = \frac{\lambda_L(o)}{\sqrt{1 - \left(\frac{T_0}{T_C}\right)^P}} \tag{2}$$

$\lambda_L(o)$ is the London penetration length at $T_0 = 0$ K, $P = 4$, and $T_C = 92$ K is the superconducting critical temperature. Where, the frequency when ε is 0 is called the ETF, which is represented by f_{th}. The thickness of $YaBa_2Cu_3O_7$ in the AFS and the host structure is different, respectively 32 nm and 1200 nm.

In the case of the ultra-low temperature, the effects of the thermal expansion coefficients and thermo-optic coefficients are also considered [22,23],

$$n^* = n + an\Delta T \tag{3}$$

$$d^* = d + bd\Delta T \tag{4}$$

In which, n and d are the refractive index and thickness at room temperature, and n^* and d^* are the refractive index and thickness at ultra-low temperature. a is the thermo-optic coefficient of the medium. For SiO_2, a is $a_1 = 6.8\times10^{-6}/^oC$. b is the thermal expansion coefficient of the medium. For SiO_2 and $YaBa_2Cu_3O_7$ [22], b are $b_1 = 2.6\times10^{-6}/^oC$ and $b_4 = 2\times10^{-5}/^oC$. In the absence of special instructions, the operating temperature T_0 is 50 K, and ΔT refers to the difference from room temperature.

The connection between different media layers is achieved through the transfer matrix method [24,25]. Under normal circumstances, when the transmittance of the OPP structure is higher than −3 dB, the human eye can see clearly, and when the transmittance is lower than −10 dB, the human eye is difficult to recognize, so based on this actual situation, *RC* can be defined as the ratio of the bandwidth of −3 dB to the bandwidth of −10 dB.

3. Analysis and discussion

Fig. 2 shows the basic principle of the angle selection structure. In Fig. 2(a), the ETF occurs at 227 THz. For the convenience of the display, the region higher than f_{th} is called the high-frequency region, while that lower than f_{th} is the low-frequency region. Accordingly, in Fig. 2(b), the superconducting layer shows transmission in the high-frequency region and reflection in the low-frequency region, which is a kind of APC. For traditional materials, the transmission phenomenon is usually displayed at the ETF, and the reflection or absorption phenomenon is usually displayed outside the ETF. We believe that this APC phenomenon of superconductors is also understandable. This is mainly due to the lossless characteristics of the superconductor, in the high-frequency region, ε is a pure real number, and the electromagnetic wave can penetrate, while in the low-frequency region, ε is a pure imaginary number, so the electromagnetic wave is reflected. Traditional materials usually have obvious imaginary parts, so electromagnetic waves are difficult to be completely transmitted, but at ETF, the optical path difference is 0, and electromagnetic waves can be transmitted. In addition, the APC phenomenon is also related to the thickness of $YaBa_2Cu_3O_7$ d_Y. If d_Y is 200 nm, the transmission performance of the superconducting layer is adjusted smoothly. And when d_Y gradually aggrandizes, the edge of the transmission window becomes steeper. Predictably, if the discussion of the frequency domain is transferred to the angle domain, the influence of thickness on the *RC* of the transmission window will also be remarkable.

In Fig. 2(c), it is clear that the angular region is divided into a high-transmission region and a high-reflection region due to the presence of APC. When d_Y is 200 nm, 400 nm, 800 nm, and 1200 nm, the *RC* values are successively 0.79, 0.86, 0.93, and 0.96. It can be observed that the increase in thickness significantly improves the selectivity of the angle window, making the division of the high-transmission region and the high-reflection region more obvious. The steeper the angle window, the

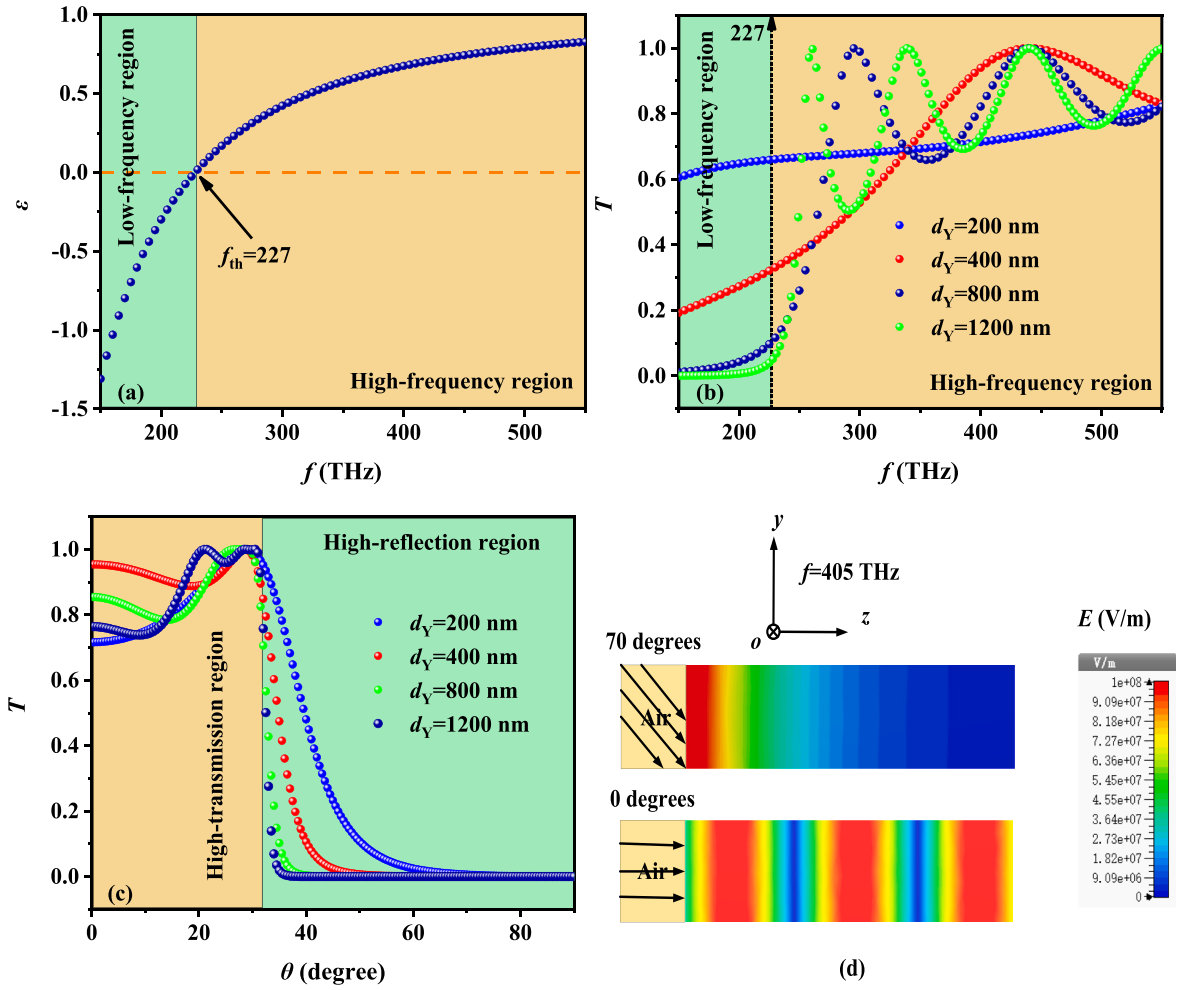

Fig. 2. (a) The distribution of dielectric constant of $YaBa_2Cu_3O_7$ with variation of frequency. (b) The effects of the thickness of $YaBa_2Cu_3O_7$ d_Y on transmittance at ETF with $\theta = 0°$. (c) The effects of thickness on transmittance of $YaBa_2Cu_3O_7$ in the angular domain with $f = 405$ THz. (d) Electric field energy distribution at $f = 405$ THz and $d_Y = 1200$ nm.

more secure the private information. In addition, Fig. 2(d) is exhibited to more clearly demonstrate the distribution of electric field energy as electromagnetic waves travel through the superconductor. When θ is 70°, the electric field distribution exists only on one side of the structure, which means that the electromagnetic wave energy does not pass through the structure and is completely reflected just after touching the structure. While for the vertical incidence, that is θ is equal to 0°, the electromagnetic waves can pass through the superconductor smoothly, leading to the result that the electric field is distributed throughout the entire structure.

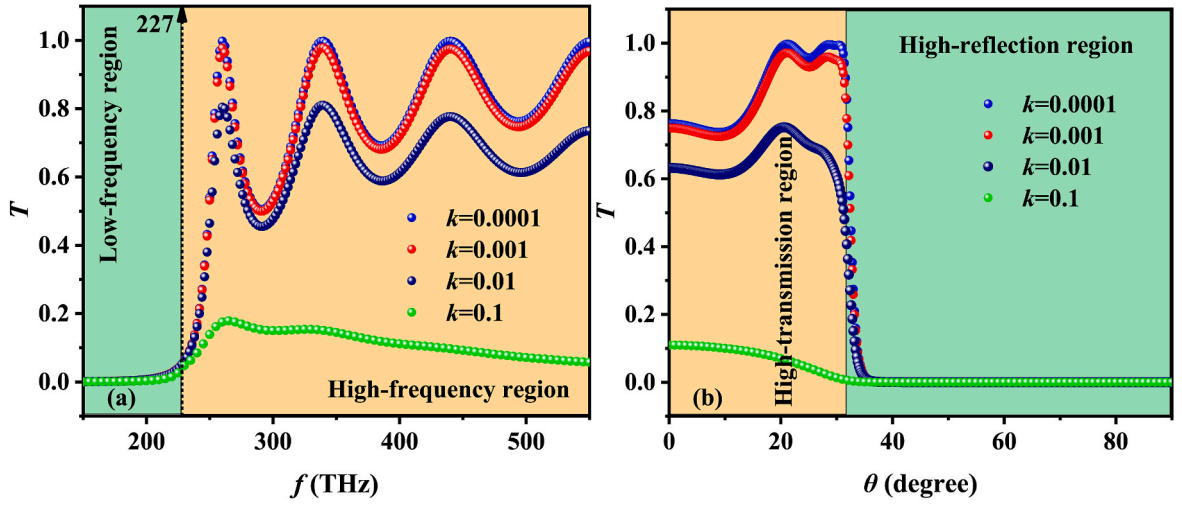

Fig. 3. (a) The effects of extinction coefficient k on transmittance at ETF with $\theta = 0°$. (b) The effects of k on transmittance in the angular domain with $f = 405$ THz.

From the above analysis, it can be inferred that APC may also exist for other materials with dielectric constant distribution similar to Fig. 2 (a), but it will be affected by the imaginary part. Therefore, extinction coefficient k is introduced on the basis of dielectric function of $YaBa_2Cu_3O_7$ to discuss the effect of imaginary part on APC properties. In Fig. 3 (a), the energy in the low-frequency region is always reflected as k increases. And the transmittance in the high-frequency region is decreasing. When k increases from 0.0001 to 0.001, APC decreases insignificantly, while when k changes from 0.01 to 0.1, APC decays rapidly and almost disappears. In Fig. 3(b), a similar phenomenon occurs for the angle domain. The highly-reflection region is not affected by k, while the highly transmitted region weakens as k increases until angle selectivity is difficult to form. It can be concluded that for media with similar dielectric function distribution, such as ferrite, InSb, plasma, angle selectivity will also exist, but the effects of the imaginary part must be controlled.

Fig. 4 is explained in terms of impedance matching principles and highlights the role of AFS. The normalized surface impedance is defined as the ratio of the impedance of the entire structure to the impedance of the vacuum wave [26]:

$$Z_{\text{eff}} = \frac{Z_{\text{d}}}{Z_0} = z_{r,\text{eff}} + jz_{i,\text{eff}} \tag{5}$$

In which, $Z_0 = |E_0|/|H_0| = (\mu_0/\varepsilon_0)^{1/2}$ is the vacuum wave impedance, whose value is about 377 Ω. $Z_{\text{d}} = |E|/|H| = (\mu/\varepsilon)^{1/2}$ is the effective impedance of the entire structure. After analysis, when the real part and imaginary part of normalized surface impedance are close to 1 and 0, respectively, the impedance matching degree is the best, and at this time the reflection can be suppressed to the greatest extent. In Fig. 4(a), when relying solely on the superconductor layer, in the range of −30∼30°, the normalized effective surface impedance value is far away from 1, proving that the impedance is mismatched and the electromagnetic wave is reflected a large extent. Adding the AFS, the real part of the normalized effective surface impedance approaches 1 within the same angle range, indicating that with impedance matching well, making remarkable transmission performance. In Fig. 4(b), the specific transmission performance is highly consistent with the results of impedance analysis, and the introduction of AFS prompts the transmission performance to be increased from 0.7 to more than 0.9.

Fig. 5 illustrates the necessity of the prism device as the background medium. In Fig. 5(a), in the entire visible light region, the angle window gradually expands from −52.6–52.6° to −70.6–70.6° with the increase of the frequency. However, for OPP devices, the angle window is too large, which greatly boosts the risk of information leakage. Considering that the superconductor film is temperature-sensitive, temperature control methods are tried to regulate the angle window in Fig. 5(b). When the frequency is 405 THz, the starting point of the red light band, the angle also faces the tendency of diffusion as the temperature varies from 0 K to 80 K. And in the range of 0∼50 K, the angle change is very weak. Even if the temperature approaches 0 K, the minimum angle area is −50.9–50.9°, which fails to meet the needs of OPP. Through the above analysis, it can be seen that it is difficult to reduce the angle window according to the inherent characteristics of the structure. Consequently, adjusting the background media is considered. Compared to the original air background, the prism is a kind of high refractive index glass, causing the optical path of the electromagnetic wave propagating through the prism enhanced. Without a prism, the structure is impedance matched to the air background, while with a prism, the original structure needs to be impedance matched to the background medium prism, which significantly reduces the range of angle matching. Therefore, in Fig. 5(c), if the frequency is climbed from 405 THz to 790 THz, the angle range is changed from −31.7–31.7° to −39.3–39.3°, and the transition area is also reduced from the original 18°–7.6°, meeting the current needs for narrow-angle protection.

In Fig. 6, the OPP characteristics in the visible band are discussed. Visible light can be divided into seven colors, corresponding to seven frequency bands. They are red (405–480 THz), orange (480–510 THz), yellow (510–530 THz), green (530–600 THz), blue (600–620 THz), indigo (620–680 THz) and violet (680–790 THz). From the perspective of OPP demand, a transmittance of more than 0.9 will not pose a health threat to human eyes, while a transmittance of less than 0.1 is difficult to observe. In Fig. 6(a), when the incident frequencies are successively 405 THz, 480 THz, 510 THz, 530 THz, 600 THz, 620 THz, 680 THz, and 790 THz, angles with a transmittance of 0.9 are respectively ±31.7°, ±34.4°, ±35.2°, ±35.7°, ±36.9°, ±37.2°, ±37.9°, ±38.8° and angles with a transmittance of 0.1 are respectively ±33.7°, ±35.8°, ±36.4°, ±36.8°, ±37.8°, ±38°, ±38.5°, ±39.3°. It can be seen that across the entire visible light region, the transmittance within ±30° is higher than 0.9, while the transmittance beyond ±40° is lower than 0.1. This also means that the proposed OPP structure can achieve full protection for areas beyond ±40° and partial protection for areas beyond ±30°. In Fig. 6(b), the distribution of RC and T values for the various color bands in the visible area are 0.97 and 0.93, 0.98 and 0.97, 0.98 and 0.96, 0.98 and 0.97, 0.98 and 0.96, 0.99 and 0.95, 0.99 and 0.96, 0.99 and 0.93 respectively. The extremely high RC feature can effectively improve the anti-voyeurism performance, and the high transmittance can greatly reduce the damage of the screen to the eyes. To visually demonstrate the anti-voyeurism effectiveness, Fig. 6(c) is illustrated. The yellow part is

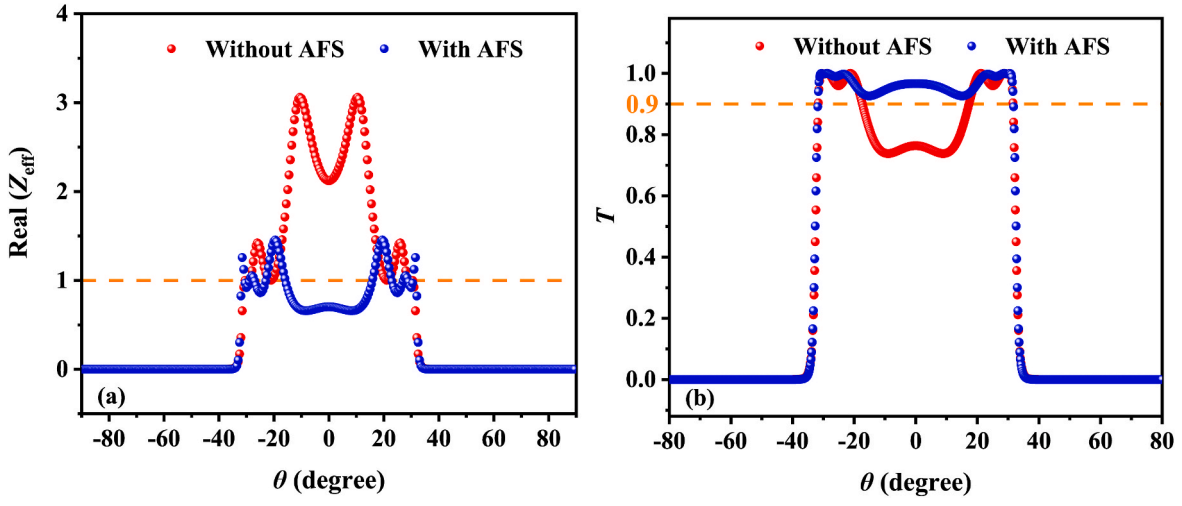

Fig. 4. At f = 405 THz, the influences of AFS, those are $(YaBa_2Cu_3O_7{\cdot}SiO_2)^2$ and $(SiO_2{\cdot}YaBa_2Cu_3O_7)$), on (a) impedance matching characteristics and (b) angle selectivity.

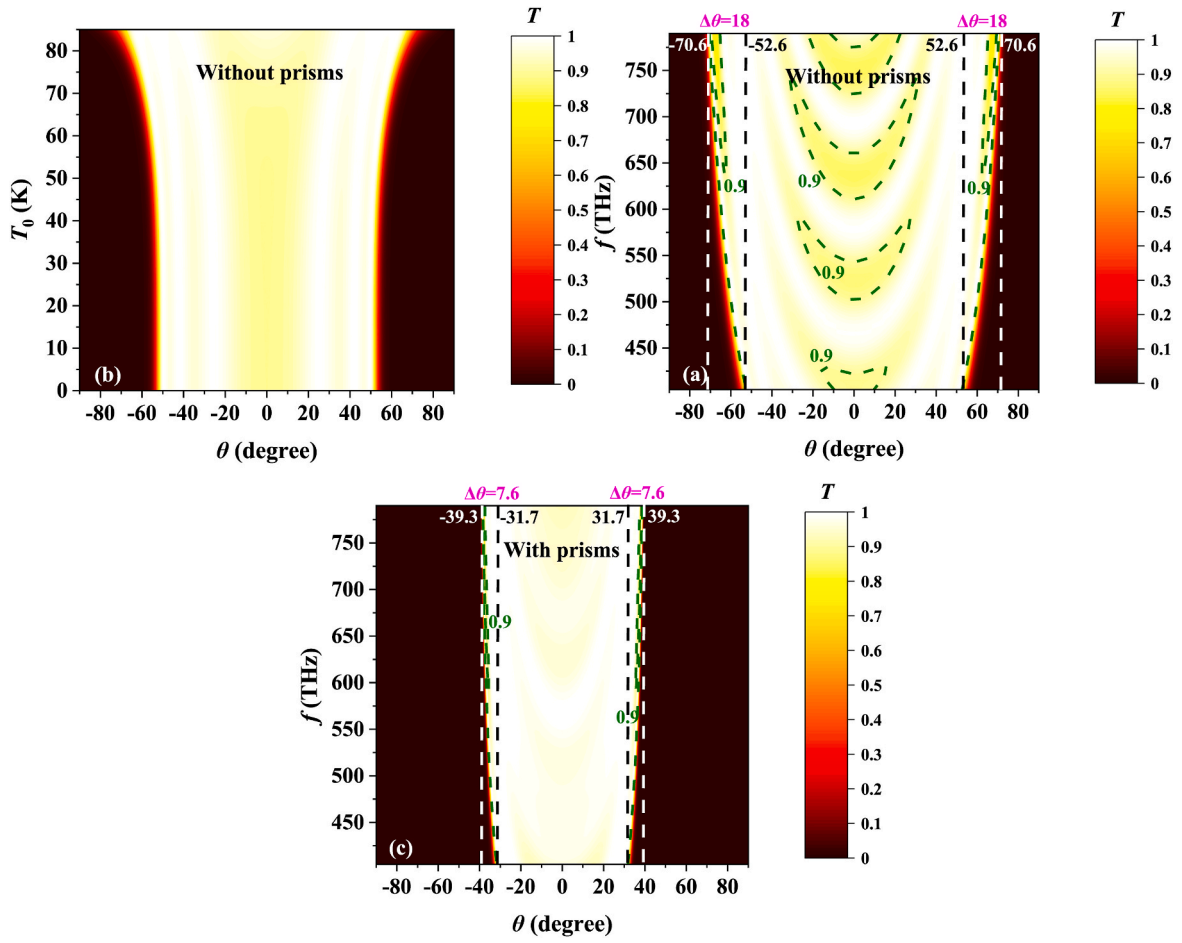

Fig. 5. (a) At $T_0 = 50$ K, OPP phenomenon without prisms. (b) At $f = 405$ THz, the effects of T_0 on regulating OPP window without prisms. (c) At $T_0 = 50$ K, OPP phenomenon with prisms. The dashed lines in dark green are contours with a transmittance of 0.9. (For interpretation of the references to color in this figure legend, the reader is referred to the Web version of this article.)

the visible area where all light has high transmittance, the green part is the transition area where some light is visible, and the blue part is the protected area where all light is invisible.

Dielectric loss is an important factor that threatens the performance of devices [27]. However, for the proposed structure, the loss of the superconductor is negligible at temperatures below the threshold. In the visible light band, the loss of SiO_2 is also very weak, and the SiO_2 layer acts as an auxiliary role of the AFS, so the impact of the loss can be almost ignored. In view of the fact that the thickness of the multilayer film structure deviated during processing, the effects of error coefficient σ on OPP are explored. According to the current technology level, a 5 % error is introduced. For ease of analysis, the error coefficient σ is defined as the error generated by the thickness of each layer of the structure. In Fig. 7(a), $\sigma = 0.95$, if seven different colors of the light wave are incident, the angular positions of transmittance equal to 0.9 change form $\pm 31.6^\circ$ to $\pm 38.7^\circ$, and angles with a transmittance of 0.1 belong to $\pm 33.8 \sim \pm 39.3^\circ$. In Fig. 7(b), $\sigma = 1.05$, for the same incident frequency points, the high transmittance angles range from $\pm 31.8^\circ$ to $\pm 37.5^\circ$, and low transmittance angles are $\pm 33.6 \sim \pm 39.2^\circ$. The corresponding resonance angle is slightly shifted, but within $\pm 30^\circ$, the transmittance of the visible area is still higher than 0.9. As for beyond $\pm 40^\circ$, the transmittance still tends to be 0. As a result, it can be inferred that thickness machining errors within a certain range will not affect the performance of OPP.

4. Conclusion

In general, in this paper, a multi-layer OPP structure based on the APC at ATF is proposed. Combining the lossless superconducting ceramic material, AFS, and prism background medium, not only does the proposed OPP structure avoids the low transmittance and low *RC* characteristics of the ultra-fine blinds, but also it overcomes the narrow band characteristics of the PCs structure. It is reasonable to draw the conclusion that for the TM wave, in the whole visible light band, *RC* values are higher than 0.97. The area within $\pm 30^\circ$ is a visible area with a transmittance higher than 0.93, while the areas beyond $\pm 40^\circ$ are completely protected areas with a transmittance tending to 0, and the other angle areas are partially protected areas. Additionally, ±5 % thickness errors are taken into account, and the results show that the OPP performance can still be maintained.

CRediT authorship contribution statement

Baofei Wan: Data curation, Formal analysis, Investigation. Haining Ye: Writing - original draft, Visualization. Yiming Ma: Writing - original draft, Visualization. Haifeng Zhang: Conceptualization, Methodology, Supervision, Writing - review&editing.

Funding

This work was supported by the Postgraduate Research & Practice Innovation Program of Jiangsu Province (Grant No. KYCX23_1004).

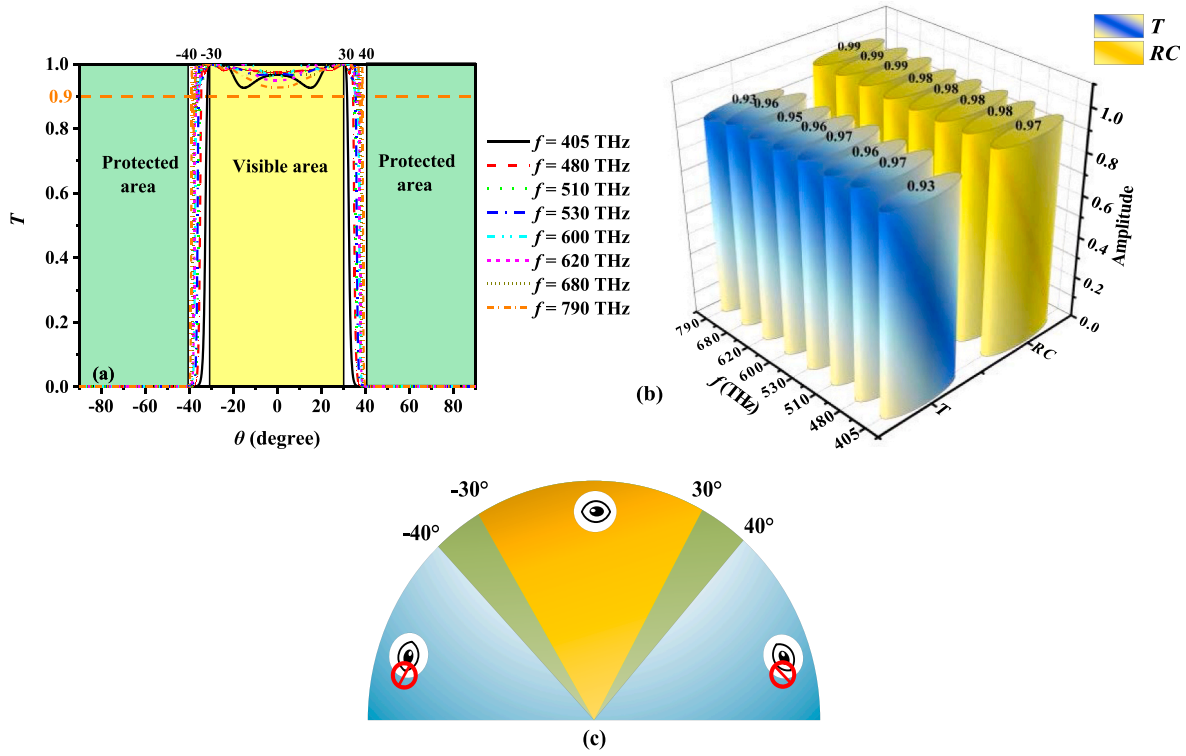

Fig. 6. (a) Analysis of OPP characteristics in visible light band. (b) The T values within ±30° and RC values of various frequencies of light. (c) Privacy protection diagram.

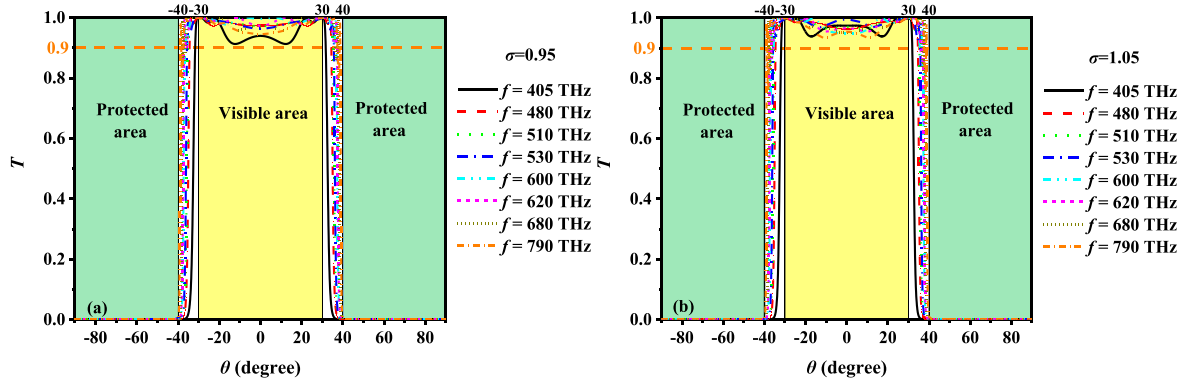

Fig. 7. Effects of thickness error factor σ on OPP performance. (a) $\sigma = 0.95$, (b) $\sigma = 1.05$.

Declaration of competing interest

This manuscript has not been published yet and not even under consideration for publication elsewhere. The authors are grateful who have participated in this research work. The authors declare no conflict of interest.

References

[1] J.I. Baek, Y.H. Kwon, J.C. Kim, T.H. Yoon, Dual-mode switching of a liquid crystal panel for viewing angle control, Appl. Phys. Lett. 90 (2007) 3895.
[2] Y.J. Lim, J.H. Kim, J.H. Her, K.H. Park, J.H. Lee, B.K. Kim, W. Kang, G. Lee, S. H. Lee, Viewing angle switching of liquid crystal display using fringe-field switching to control off-axis phase retardation, J. Phys. D Appl. Phys. 43 (2010) 85501–85506.
[3] G.J. Woodgate, M.G. Robinson, E. Sommerlade, Late-news poster: intelligent backlight technology developments for uniformity, privacy & 3D operation, SID Sympos. Digest Tech. Pap. 46 (2015) 1448–1451.
[4] M.G. Robinson, G.J. Woodgate, J. Harrold, Switchable privacy display design and optimisation, SID Symposium: Dig. Technol. Pap. 49 (2018) 1567–1570.
[5] J. Ishii, G. Saito, M. Imai, F. Okumura, Late-news paper: liquid crystal privacy-enhanced displays for mobile PCs, SID symposium, Dig. Technol. Pap. 1 (2009) 15.
[6] S. Aguinaga, C. Poellabauer, Method for Privacy-Protecting Display and Exchange of Emergency Information on Mobile Devices, 2012 International Conference on Collaboration Technologies and Systems (CTS), IEEE, 2012, pp. 596–599.
[7] A. Christ, S.G. Tikhodeev, N.A. Gippius, J. Kuhl, H. Giessen, Waveguide-plasmon polaritons: strong coupling of photonic and electronic resonances in a metallic photonic crystal slab, Phys. Rev. Lett. 91 (2003), 183901.
[8] M. Kamran, M. Faryad, Excitation of surface plasmon polariton waves along the direction of periodicity of a one-dimensional photonic crystal, Phys. Rev. A 99 (2019) 53811, 53811.
[9] C. Zhou, Y. Qi, S. Zhang, W. Niu, S. Wu, W. Ma, B. Tang, Water rewriteable double-inverse opal photonic crystal films with ultrafast response time and robust writing capability, Chem. Eng. J. 439 (2022) 439.
[10] S. Wu, J. Nan, Y. Wu, Low-angle-dependent anticounterfeiting label decoded by alcohol tissue wiping based on a multilayer photonic crystal structure, ACS Appl. Mater. Interfaces 23 (2022) 14.
[11] H. Iizuka, N. Ngheta, E. Sugiura, Extremely small wavevector regime in a one-dimensional photonic crystal heterostructure for angular transmission filtering, Opt. Lett. 41 (2016) 3829–3832.
[12] B.F. Wan, H.N. Ye, D. Zhang, H.F. Zhang, A variable refractive index sensor based on epsilon-near-zero spatial selection structure and its potential in biological detection, New J. Phys. 25 (2023), 023003.

[13] H. Tanaka, I. Takai, H. Fujikawa, H. Iizuka, Nearly polarization-independent angular filters consisting of one-dimensional photonic crystals realized in the visible region, J. Lightwave Technol. 36 (2018) 2517–2523.
[14] Y. Shen, Metamaterial broadband angular selectivity, Phys. Rev. B 90 (2014), 125422.
[15] H. Huang, Z.X. Shen, Angle-selective surface based on uniaxial dielectric-magnetic slab, IEEE Antenn. Wirel. PR 19 (2020) 2457–2461.
[16] A. Alu, G.D. Aguanno, N. Mattiucci, M.J. Bloemer, Plasmonic Brewster angle: broadband extraordinary transmission through optical gratings, Phys. Rev. Lett. 106 (2011), 123902.
[17] J. Münzberg, A. Vetter, F. Beutel, W. Hartmann, S. Ferrari, Wolfram H.P. Pernice, C. Rockstuhl, Superconducting nanowire single-photon detector implemented in a 2D photonic crystal cavity, Optica 5 (2018) 658–665.
[18] A.H. Aly, F.A. Sayed, THz cutoff frequency and multifunction Ti2Ba2Ca2Cu3O10/GaAs photonic bandgap materials, Int. J. M.Phys. B 34 (2020), 30462.
[19] C.A. Hu, J.W. Liu, C.J. Wu, T.J. Yang, S.L. Yang, Effects of superconducting film on the defect mode in dielectric photonic crystal heterostructure, Solid State Commun. 157 (2013) 54–57.
[20] M.S. Chen, C.J. Wu, T.J. Yang, Investigation of optical properties in near-zero-permittivity operation range for a superconducting photonic crystal, Appl. Phys. A 104 (2011) 913–919.
[21] B.J. Frey, J.B. Heaney, L.G. Burriesci, D.B. Leviton, T.J. Madison, Q. Gong, M. Tecza, Cryogenic temperature-dependent refractive index measurements of N-BK7, BaLKN3, SF15, and E-SF03, Proc. SPIE 6692 (2007), 669205.
[22] A.H. Alya, S.E.S. Abdel Ghany, B.M. Kamal, D. Vigneswaran, Theoretical studies of hybrid multifunctional $YaBa_2Cu_3O_7$ photonic crystals within visible and infra-red regions, Ceram. Int. 46 (2020) 365–369.
[23] J.Y. Lin, M. Gurvitch, S.K. Tolpygo, A. Bourdillon, S.Y. Hou, J. M Phillips, Flux pinning in YaBa2Cu3O7-δ thin films with ordered arrays of columnar defects, Phys. Rev. B 54 (1996) 717.
[24] L.M. Qi, Z.Q. Yang, F. Lan, X. Gao, Z.J. Shi, Properties of obliquely incident electromagnetic wave in one-dimensional magnetized plasma photonic crystals, Phys. Plasmas 17 (2010), 042501.
[25] I.V. Timofeev, D.N. Maksimov, A.F. Sadreev, Optical defect mode with tunable Q factor in a one-dimensional anisotropic photonic crystal, Phys. Rev. B 97 (2018), 024306.
[26] T.W. Chang, C.H. Huang, D.J. Hou, C.J. Wu, D.X. Chen, Analysis of unidirectional absorption in a defective superconducting photonic crystal, IEEE Photon. J. 9 (2017), 5900509.
[27] H. Li, H. Zhou, G. Wei, H. Xu, M. Qin, J. Liu, F. Wu, Photonic spin-selective perfect absorptance on planar metasurfaces driven by chiral quasi-bound states in the continuum, Nanoscale 15 (2023) 6636–6644.